Gate Optimization of NEQR Quantum Circuits via PPRM Transformation

Shahab Iranmanesh[1], Hossein Aghababa[2], and Kazim Fouladi[3]

[1]School of Electrical and Computer Engineering, College of Engineering, University of Tehran, Tehran, Iran , shahab.iranmanesh@ut.ac.ir
[2]Department of Engineering, Loyola University Maryland, Maryland, USA, Founder of Quantum Computation and Communication Laboratory, University of Tehran, Tehran, Iran
[3]Faculty of Engineering, College of Farabi, University of Tehran, Tehran, Iran

Abstract

Quantum image representation (QIR) is a key challenge in quantum image processing (QIP) due to the large number of pixels in images, which increases the need for quantum gates and qubits. However, current quantum systems face limitations in run-time complexity and available qubits. This work aims to compress the quantum circuits of the Novel Enhanced Quantum Representation (NEQR) scheme by transforming their Exclusive-Or Sum-of-Products (ESOP) expressions into Positive Polarity Reed-Muller (PPRM) equivalents without adding ancillary qubits. Two cases of run-time complexity—exponential and linear— are considered for NEQR circuits with m controlling qubits ($m \rightarrow \infty$), depending on the decomposition of multi-controlled NOT gates. Using nonlinear regression, the proposed transformation is estimated to reduce the exponential complexity from $O(2^m)$ to $O(1.5^m)$, with a compression ratio approaching 100%. For linear complexity, the transformation is estimated to halve the run-time, with a compression ratio approaching 52%. Tests on six 256×256 images show average reductions of 105.5 times for exponential cases and 2.4 times for linear cases, with average compression ratios of 99.05% and 58.91%, respectively.

Keywords: Quantum Image Representation, NEQR, Quantum Image Compression, Multi Controlled-NOT gates, Exclusive-Or Sum-of-Products (ESOP), Optimization, Minimization, Positive Polarity Reed-Muller (PPRM), Nonlinear Regression

1 Introduction

Limitation is a concept intertwined with today's quantum computers, preventing them from becoming general-purpose machines and substituting digital computers. The noisy intermediate-scale quantum (NISQ) era has been marked by a limited number of qubits, a noisy and error-prone environment, and quantum decoherence, all of which restrict the design of quantum circuits in terms of execution time. Consequently, optimizing the run-time complexity of quantum circuits by reducing the number of quantum gates and changing their types is both significant and necessary.

Quantum image representation (QIR), which involves encoding digital images into quantum circuits, is a subfield of quantum image processing (QIP) that faces run-time challenges due to the large and increasing number of pixels in modern images and videos. Various QIR models have been proposed, including Qubit Lattice [1], Real Ket [2], entangled images [3], and a Flexible Representation of Quantum Images (FRQI), which encodes pixel grayscale values into a grayscale qubit by

1

mapping each pixel value to an angle [4]. Other models include an RGB Multi-Channel Representation for Quantum Images (MCQI) [5] and a Novel Enhanced Quantum Representation (NEQR) [6], which is similar to classical image representation and facilitates classically inspired arithmetic operations, with the potential for processing quantum operations on all pixels simultaneously due to the quantum mechanics superposition phenomenon. Among these models, FRQI and NEQR are more commonly used, and some representations have been developed based on these two, such as an improved FRQI model (FRQCI) [7], Improved NEQR (INEQR) [8], a Generalized Quantum Image Representation (GQIR) [9], and a Generalized model of NEQR (GNEQR) [10].

To decrease the run-time complexities of QIR schemes, researchers have proposed various optimizations and compressions, referred to as quantum image compressions (QICs). QIC aims to reduce the quantum resources required for QIR by compressing a digital image before constructing its quantum circuit, lowering the number of quantum gates, and simplifying quantum gates [11]. A few QICs have been proposed, such as a hybrid quantum vector quantization encoding algorithm [12], using the Quantum Discrete Cosine Transform (QDCT) [13], image compression based on the Functional Sized Population Quantum Evolutionary Algorithm (FSQEA) [14], an algorithm using Quantum Backpropagation (QBP) [15], employing Grover's quantum search algorithm [16], the DCT-GQIR method which uses Direct Cosine Transform preparation and GQIR encoding inspired by JPEG image compression [17], applying compression to quantum RGB images using the quantum Haar wavelet transform (HQWT) and iterative quantum Fibonacci transform (IQFT) [18], a quantum version of an autoencoder based on parameterized quantum circuits [19], and an image compression and reconstruction algorithm leveraging the quantum network (QN) and the gradient descent algorithm [20]. Other QICs focus on minimizing QIR or both image compression and QIR minimization. Enhanced FRQI (EFRQI) minimizes GQIR representation using auxiliary qubits [21], while the DCT-EFRQI scheme compresses images and minimizes their QIRs [22]. This present work aims to optimize NEQR quantum circuits without any compression before the quantum representation stage.

An NEQR circuit consists of a collection of quantum logic multi-controlled NOT (MCNOT) gates, mapping the circuit's output to Exclusive-Or Sum-of-Products (ESOP) expansions. Some works suggest using the Espresso algorithm [23] for minimizing the ESOP expressions resulting from an NEQR quantum circuit [6][24][25]. However, the Espresso algorithm is best suited for minimizing Boolean functions in the form of Sum-of-Products (SOP). To minimize the ESOP expressions resulting from an NEQR circuit using Espresso, an additional process is required to convert the minimized result into ESOP form. Many methods have been introduced to optimize ESOP expressions directly, which are either exact or heuristic, including a nonlinear integer programming approach [26], a parallel algorithm [27], using ordered Kronecker functional decision diagrams [28], fast heuristic minimization [29], and Karnaugh Maps [30][31].

In this work, transforming ESOP expressions, resulting from implementing NEQR circuits, to Positive Polarity Reed-Muller (PPRM) expressions without further optimization is investigated. Furthermore, to measure and compare the run-time complexities of non-optimized NEQR circuits and their optimized versions, the concept of quantum cost (QC) is defined based on the number of primitive quantum gates, such as the CNOT gate, whose QC is considered 1. Two cases of compression rate and QC optimization rate are explored for images optimized by the PPRM transformation and are estimated using nonlinear regression to derive mathematical functions that verify their growth as the number of pixels increases. To promote transparency, the source code is available on GitHub at `https://github.com/shahab-iranmanesh/PPRM_Optimization_of_NEQR`.

The rest of this report is organized as follows: Section 2 discusses two kinds of MCNOT gates, NEQR representations, and PPRM expressions. Section 3 describes two algorithms for transforming ESOP expressions into PPRM ones, which are used in Section 4 to explore the optimization and compression rates for real and random images. Finally, Section 5 offers some concluding remarks.
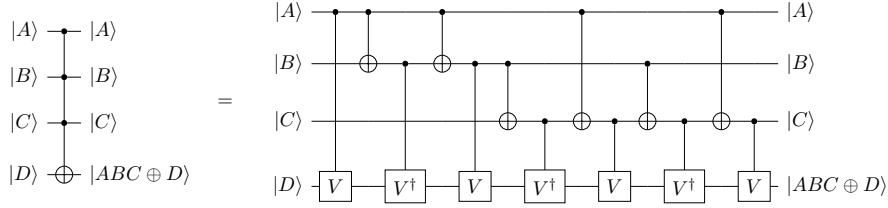
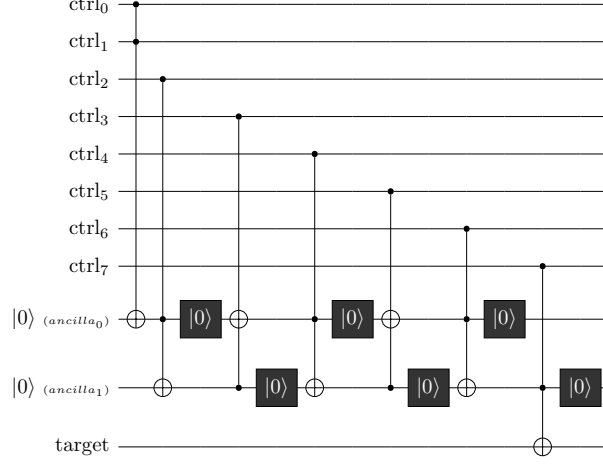Figure 1: Quantum circuit of the $C^3(X)$ gate without ancillary qubits [32]

Figure 2: Quantum circuit of the proposed $C_R^8(X)$ gate using two ancillary qubits

2 Background

2.1 Multi-Controlled NOT (MCNOT) gate

The MCNOT gate, also referred to as $C^m(X)$ in this paper, where $X = \begin{pmatrix} 0 & 1 \\ 1 & 0 \end{pmatrix}$, is a controlled Pauli-X gate with $m \geq 2$ control qubits and one target qubit. When all its control qubits are in the state $|1\rangle$, the target qubit is flipped; otherwise, the target qubit retains its initial state. Various methods have been proposed to implement the $C^m(X)$ gate in quantum circuits, as it is not a universal basis gate for quantum systems, unlike the CNOT gate. In this paper, two designs of the $C^m(X)$ gate are considered for simulation and analysis. One design, shown in Figure 1 and described in [32], does not use any additional ancillary qubits and has an exponential quantum cost (QC) of $3 \times 2^m - 4$, as calculated in [31]. The other design, proposed in [31] and shown in Figure 2, is called the MCNOT with Reset (MCNOT-R or $C_R^m(X)$), which utilizes a *reset* operation (represented by black boxes with $|0\rangle$) to reuse its two ancillary qubits and has a QC of $19m - 32$.

Applying each $C^m(X)$ or $C_R^m(X)$ gate with control qubits $\{ctrl_i\}_{i=0}^{m}$ on a target qubit t, results in a state $|t\rangle = |\prod_{i=0}^{m} ctrl_i \oplus t\rangle$, where $\prod_{i=0}^{m} ctrl_i$ is the AND of the Boolean variables $\{ctrl_i\}_{i=0}^{m}$. For example, if the initial state of the target qubit is set to $|0\rangle$, applying five MCNOT gates results in the target qubit being in a state equivalent to the XOR of five product terms, each of which is the product of the control qubits' states of each MCNOT gate. This type of expression is called an Exclusive-Or Sum-of-Products (ESOP), as seen in the NEQR quantum circuits described in the next subsection.

3

2.2 NEQR

A Novel Enhanced Quantum Representation (NEQR) model [6] was proposed by Zhang et al. to represent a digital grayscale image using a quantum circuit with two groups of entangled qubits: one group for the grayscale values of the pixels and another for the coordinates that provide positional information for all the pixels simultaneously. A $2^n \times 2^n$ digital image with grayscale values in the range $[0, 2^q - 1]$ is represented by a normalized superposition of tensor products of quantum states, as expressed by Equation 1, where $|C_i^{YX}\rangle$ represents the ith qubit of the q-qubit grayscale value associated with the pixel at vertical coordinate Y and horizontal coordinate X.

$$|image\rangle = \frac{1}{2^n} \sum_{Y=0}^{2^n-1} \sum_{X=0}^{2^n-1} \bigotimes_{i=0}^{q-1} |C_i^{YX}\rangle |Y\rangle |X\rangle \tag{1}$$

When a grayscale bit of an image at a specified pixel is 1, the corresponding qubit must be flipped from its initial value $|0\rangle$ to $|1\rangle$. Figure 3 shows an example of a 2×2 grayscale image, its NEQR expression, and the corresponding quantum circuit. As illustrated, for each grayscale qubit $|C_i^{YX}\rangle$, several $C^2(X)$ (Toffoli) gates are applied under the control of Y and X qubits. Each of these control qubits is placed into an equal superposition of $|0\rangle$ and $|1\rangle$ by a Hadamard gate $H = \frac{1}{\sqrt{2}} \begin{pmatrix} 1 & 1 \\ 1 & -1 \end{pmatrix}$ before controlling the Toffoli gates. For example, the grayscale value of $|C_0^{YX}\rangle$ is $|1\rangle$ only when $|YX\rangle = |11\rangle$. In this case, a single Toffoli gate is required, controlled by Y and X qubits in their positive state. Thus, if the superposition of the coordinate qubits is measured and the result is 11, the value of $|C_0^{YX}\rangle$ is expected to be 1 after measurement.

The larger an image is, the more coordinate qubits are required, necessitating the use of MCNOT gates with more than two control qubits. For an NEQR circuit representing a $2^n \times 2^n$ image, MCNOT gates with $2n$ control qubits ($C^{2n}(X)$) are needed. Consequently, such quantum circuits can have a high run-time complexity, with either exponential or polynomial QC, making them unsuitable for the coherence times of current quantum systems. Therefore, optimizing NEQR circuits is essential.

2.3 Positive Polarity Reed-Muller (PPRM) Expressions

ESOP expressions, also known as Reed-Muller (RM) expressions, can be optimized using various proposed methods. As an example of a two-input expression, consider the $|C_6^{YX}\rangle$ qubit in Figure 3, which has three Toffoli gates applied to it. This results in the expression $0 \oplus \overline{Y}X \oplus Y\overline{X} \oplus YX$. To optimize the gates applied to $|C_6^{YX}\rangle$, the ESOP expression $0 \oplus \overline{Y}X \oplus Y\overline{X} \oplus YX$ can be simplified to $\overline{Y}X \oplus Y$, as calculated in Equation 2. However, for a large number of inputs, manual calculation or other similar methods, such as Karnaugh maps, are impractical and do not guarantee a globally optimal solution.

$$0 \oplus \overline{Y}X \oplus Y\overline{X} \oplus YX = 0 \oplus \overline{Y}X \oplus Y(\overline{X} \oplus X) = 0 \oplus \overline{Y}X \oplus Y = \overline{Y}X \oplus Y \tag{2}$$

ESOP expressions have canonical subgroup families, as illustrated in Figure 4 [33]. In this figure, the Fixed Polarity Reed-Muller (FPRM) form is the smallest subgroup compared to other subgroups, with product terms fixed in terms of polarity. The Positive Polarity Reed-Muller (PPRM) is a form of FPRM with positive polarity, where product terms are composed of positive and non-complementary literals, as shown in Equation 4. Since the PPRM form is the smallest subgroup among these families, it is expected that NEQR circuits can be simplified by converting their Boolean functions to PPRM form.

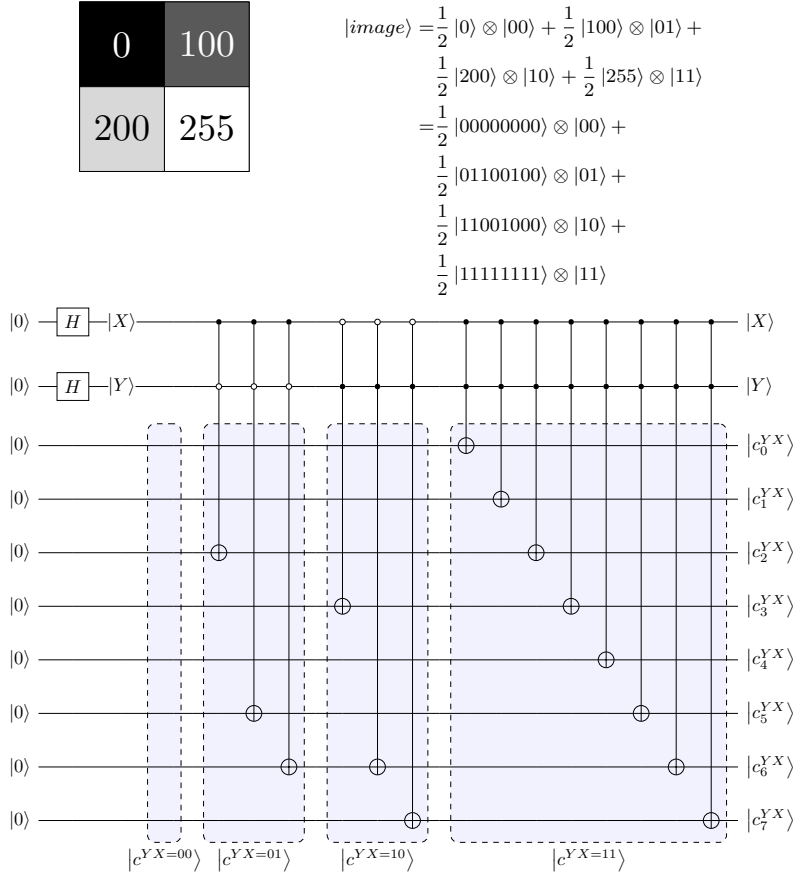$$f(x_{n-1}, x_{n-2}, \ldots, x_0) = \sum_{k=0}^{2^n-1} a_k m_k; \quad a_k \in \{0, 1\}, \quad m_k : minterm \tag{3}$$

4

Figure 3: NEQR representation and quantum circuit of a 2×2 grayscale image

$$f(x_{n-1}, x_{n-2}, \ldots, x_0) = b_0 \oplus b_1 x_0 \oplus b_2 x_1 \oplus b_3 x_1 x_0 \oplus \ldots \oplus b_{2^{(n-1)}} x_{n-1} x_{n-2} \ldots x_0; \quad b_j \in \{0, 1\} \quad (4)$$

3 PPRM transform

An algorithmic and precise method to obtain the PPRM form of a Boolean expression is described as follows [34]. A matrix named $R(n)$ is produced by the n-times Kronecker product of $R(1)$ with itself, as shown in Equation 5. Then, $X(n)$ is defined as in Equation 6, where x_i's are the inputs of the Boolean function f, as shown in Equation 3.

$$R(1) = \begin{pmatrix} 1 & 0 \\ 1 & 1 \end{pmatrix}; \quad R(n) = \bigotimes_{i=0}^{n-1} R(1) \quad (5)$$

$$X(n) = \bigotimes_{i=0}^{n-1} \begin{bmatrix} 1 & x_i \end{bmatrix} = \begin{bmatrix} 1 & x_{n-1} \end{bmatrix} \otimes \begin{bmatrix} 1 & x_{n-2} \end{bmatrix} \otimes \ldots \otimes \begin{bmatrix} 1 & x_0 \end{bmatrix}$$
$$= \begin{bmatrix} 1 & x_0 & x_1 & x_1 x_0 & x_2 & x_2 x_0 & x_2 x_1 & x_2 x_1 x_0 \ldots \end{bmatrix} \quad (6)$$

After calculating the 2^n vector $\overrightarrow{b}$, which includes the b_j coefficients used in Equation 4, the PPRM form of f can be obtained by the $*$ operation between $X(n)$ and $\overrightarrow{b}$, which multiplies each cor-

Figure 4: Set-theoretic relationships between different families of ESOP canonical forms [33]

responding element and XORs them together, as shown in Equation 7. To calculate $\overrightarrow{b}$, the $*$ operation is applied between $R(n)$ and the vector $\overrightarrow{a}$, which includes the a_k coefficients used in Equation 3.

$$\overrightarrow{b} = R(n) * \overrightarrow{a}$$

$$f = X(n) * \overrightarrow{b} = [1 \quad x_0 \quad x_1 \quad x_1 x_0 \quad \ldots] * \begin{pmatrix} b_0 \\ b_1 \\ b_2 \\ b_3 \\ \vdots \end{pmatrix} = b_0 \oplus b_1 x_0 \oplus b_2 x_1 \oplus b_3 x_1 x_0 \oplus \ldots \quad (7)$$

Bakoev et al. proposed another algorithm in [35] to calculate $\overrightarrow{b}$ with a dimension of 2^n more quickly than using $R(n)$, consuming considerably less memory. As described in Algorithm 1, the input vector $\overrightarrow{a}$ is divided into blocks of size 2^k $(k = 0, 1, \ldots, n)$ by using a dynamically changing $mask$ array, as shown in lines 4 and 5. In each iteration, a bitwise XOR operation is performed between the corresponding odd and even blocks. The result of this XOR operation is stored in the even blocks, while the odd blocks remain unchanged. This process repeats, with the block size doubling at each step.

Algorithm 1 Binary PPRM Algorithm

Require: Input array a
1: blocksize $\leftarrow 1$
2: $n \leftarrow \log_2(\text{length of } a)$
3: **for** $k = 0$ to $n - 1$ **do**
4:      mask $\leftarrow [[1] \times 2^k, [0] \times 2^k] \times 2^{n-(k+1)}$
5:      $\triangleright mask : \underbrace{111\ldots100}_{2^k}\underbrace{00\ldots0}_{2^k} \cdots \underbrace{111\ldots100}_{2^k}\underbrace{00\ldots0}_{2^k}$
6:      temp $\leftarrow$ zeros like a $\triangleright$ Array of the same size as a
7:      temp[blocksize:] $\leftarrow (a \,\&\, \text{mask})[: -\text{blocksize}]$
8:      $\triangleright$ Shift right masked a by blocksize
9:      $a \leftarrow a \oplus \text{temp}$ $\triangleright$ XOR operation between all blocks
10:      blocksize $\leftarrow 2 \times$ blocksize
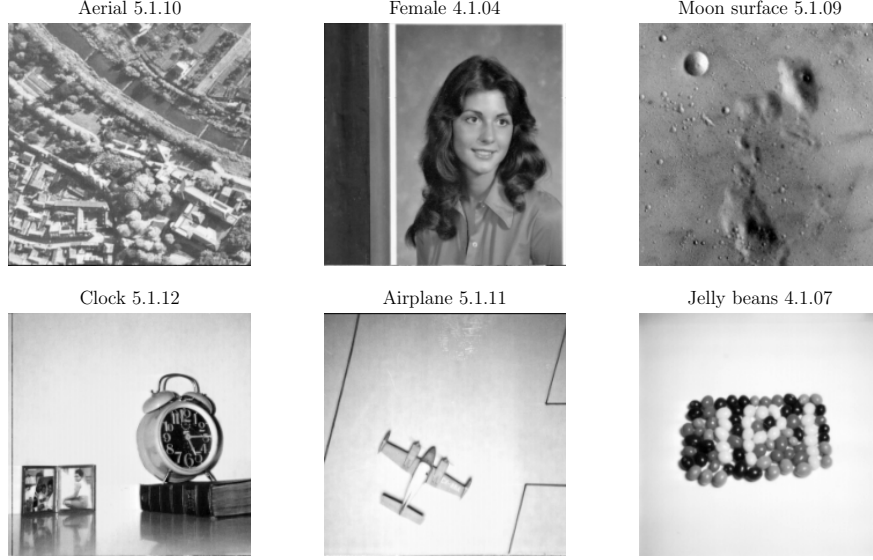11: **end forreturn** a

---

Figure 5: Six tested images, each with a resolution of 256×256

4 Simulation Results and Analysis

An experiment was conducted to test the PPRM QC optimization of the NEQR representations of six images chosen from the USC-SIPI dataset [36], each with a size of 256×256 and 256 grayscale levels: "Aerial," "Female," "Moon surface," "Clock," "Airplane," and "Jelly beans" (Figure 5). To reduce the number of control qubits in the MCNOT gates used in the NEQR circuit of each image, a 65536×8 (where $65536 = 256 \times 256$) binary matrix was prepared. Each row of this matrix corresponds to a pixel and represents its 8-bit grayscale value. Additionally, each column with index i indicates which product terms constitute the initial ESOP expression of $|C_i^{YX}\rangle$, meaning that this column indicates the coefficients of the minterms (a_k's in Equation 3) of the f function corresponding to the grayscale qubit $|C_i^{YX}\rangle$.

Each column of this matrix is then transformed into a $\overrightarrow{b}$ vector using the *Binary PPRM* function. Afterwards, the expected PPRM expression for each of the eight grayscale qubits can be obtained by applying the $*$ operation between $X(n)$ and each $\overrightarrow{b}$ vector. Then, the product terms in the i-th resulting PPRM expression are used for the controlling qubits of the new MCNOT gates applied to $|C_i^{YX}\rangle$.

Tables 1 and 2 demonstrate the reduction of QCs in each tested image using MCNOT and MCNOT-R gates, respectively, along with their compression ratios, as defined in Equation 8. On average, there is a 105.5-fold reduction in QC using MCNOT and a 2.4-fold reduction in QC using MCNOT-R. The average compression ratios are 99.05% and 58.91%, respectively.

$$Compression\,Ratio = \left(1 - \frac{QC\,of\,Optimized}{QC\,of\,NonOptimized}\right) \times 100\% \qquad (8)$$

Another experiment investigates the QC optimization rates, defined in Equation 9, and the compression ratios for images with random grayscale pixel values, ranging in size from $2^1 \times 2^1$ to $2^{11} \times 2^{11}$. These simulations were run on a system with an Intel Core i3-6100 $\times$ 4 CPU, 8 GB RAM, and Linux Ubuntu 24.04.1 LTS, and images with dimensions beyond $2^{11} \times 2^{11}$ could not be simulated due to hardware limitations. As shown in Figure 6, considering m as the number of controlling qubits ($2 \le m \le 22$), there is an exponential increase in the QC optimization rate

Image	QC of Non-Optimized	QC of Optimized	Compression Ratio
Aerial 5.1.10	53865957128	514219033	99.05%
Female 4.1.04	50562026908	508945459	98.99%
Moon surface 5.1.09	50633394160	517464591	98.98%
Clock 5.1.12	58309797340	506508163	99.13%
Airplane 5.1.11	56223632296	516989043	99.08%
Jelly beans 4.1.07	53324902920	497631277	99.07%

Table 1: PPRM QC Reductions of the NEQR Representations Using MCNOT Gates

Image	QC of Non-Optimized	QC of Optimized	Compression Ratio
Aerial 5.1.10	74523104	31476768	57.76%
Female 4.1.04	69952144	30483500	56.42%
Moon surface 5.1.09	70050880	31264133	55.37%
Clock 5.1.12	80671120	30194410	62.57%
Airplane 5.1.11	77784928	30924631	60.24%
Jelly beans 4.1.07	73774560	28723803	61.07%

Table 2: PPRM QC Reductions of the NEQR Representations Using MCNOT-R Gates

for representations using MCNOT gates, which is estimated by the function $1.33^m + 0.49$. In contrast, the optimization rate for representations using MCNOT-R gates exhibits an exponential decrease, described by the function $1.12^{-(1.60m-9.45)} + 2.10$, with the curve approaching a limit of 2.10. In addition, the compression ratios for NEQR circuits using MCNOT gates, estimated by the function $-2.43^{-(0.24m-4.54)} + 100.89$, asymptotically approach 100% as the number of qubits increases. Similarly, the compression ratios for NEQR circuits using MCNOT-R gates, estimated by $1.82^{-(0.24m-5.93)} + 52.27$, approach 52% as the number of qubits tends to infinity. These estimations were performed using the nonlinear regression *curve_fit* method from the *scipy.optimize* library in Python. Consequently, the optimized QCs have complexities of $O(1.5^m)$ and $O(9m)$ for NEQR circuits using MCNOT and MCNOT-R gates, respectively.

$$QC\,Optimization\,Rate = \frac{QC\,of\,NonOptimized}{QC\,of\,Optimized} \qquad (9)$$

5 Conclusion

This paper aims to determine whether the PPRM transformation of ESOP expressions in an NEQR quantum circuit can effectively reduce the quantum cost (QC). To achieve this, an efficient algorithm in terms of run-time and memory complexity was selected over another algorithm that uses matrix multiplication. Six 256×256 test images were transformed into binary vectors and converted to PPRM to verify their QC reductions using either MCNOT gates or MCNOT-R gates in their NEQR circuits. The results showed average QC reductions of 105.5 times for NEQR circuits with MCNOT gates and 2.4 times for NEQR circuits with MCNOT-R gates, with average compression ratios of 99.05% and 58.91%, respectively.

Additionally, images with random pixel values, with dimensions ranging from $2^1 \times 2^1$ to $2^{11} \times 2^{11}$, were analyzed to investigate their QC reductions and compression ratios. The results indicate that the optimization rate for NEQR circuits with exponential QC $O(2^m)$, which depends on the number of controlling qubits m, increases exponentially and is estimated by $O(1.33^m)$. In contrast, the
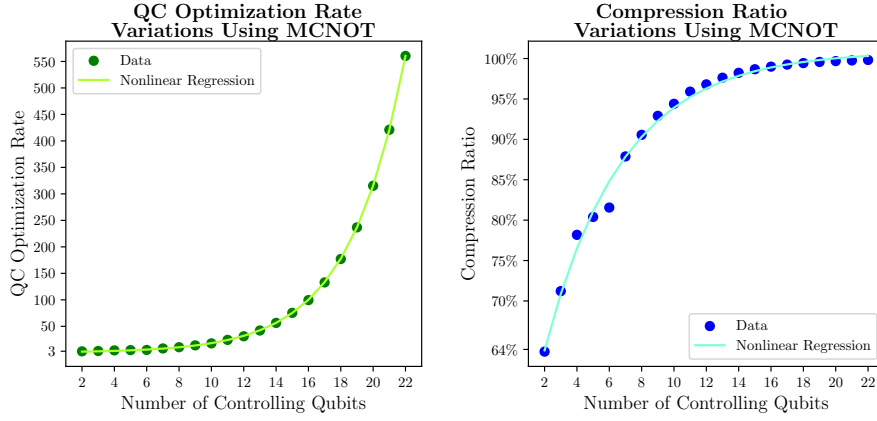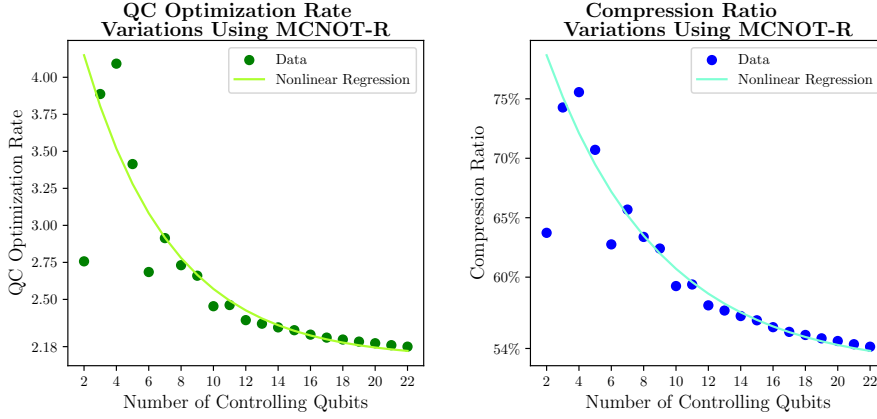
Figure 6: PPRM QC Optimization Rate and Compression Ratio for Random Images sized from $2^1 \times 2^1$ to $2^{11} \times 2^{11}$, using (a) MCNOT gates and (b) MCNOT-R gates

optimization rate for NEQR circuits with linear QC $O(m)$ decreases as the number of controlling qubits increases, approaching a constant value of 2.1. Moreover, the compression ratios tend to approach 100% for circuits using MCNOT gates and 52% for those using MCNOT-R gates.

References

[1] Salvador Venegas-Andraca and Sougato Bose. "Storing, Processing and Retrieving an Image using Quantum Mechanics". In: *Proceedings of SPIE - The International Society for Optical Engineering* 5105 (Aug. 2003). DOI: 10.1117/12.485960.

[2] Jose I. Latorre. *Image compression and entanglement*. 2005. arXiv: quant-ph/0510031 [quant-ph].

[3] S. E. Venegas-Andraca and J. L. Ball. "Processing images in entangled quantum systems". In: *Quantum Information Processing* 9.1 (2010), pp. 1–11. ISSN: 1573-1332. DOI: 10.1007/s11128-009-0123-z.

[4] Phuc Q. Le, Fangyan Dong, and Kaoru Hirota. "A flexible representation of quantum images for polynomial preparation, image compression, and processing operations". In: *Quantum Information Processing* 10.1 (2011), pp. 63–84. ISSN: 1573-1332. DOI: 10.1007/s11128-010-0177-y.

[5] Bo Sun, Abdullah Iliyasu, Fei Yan, Fangyan Dong, and Kaoru Hirota. "An RGB Multi-Channel Representation for Images on Quantum Computers". In: *Journal of Advanced Computational Intelligence and Intelligent Informatics* 17 (May 2013), pp. 404–417. DOI: 10.20965/jaciii.2013.p0404.

[6] Yi Zhang, Kai Lu, Yinghui Gao, and Mo Wang. "NEQR: a novel enhanced quantum representation of digital images". In: *Quantum Information Processing* 12.8 (2013), pp. 2833–2860. ISSN: 1573-1332. DOI: 10.1007/s11128-013-0567-z.

[7] Panchi Li and Xiande Liu. "Color image representation model and its application based on an improved FRQI". In: *International Journal of Quantum Information* 16.01 (2018), p. 1850005. DOI: 10.1142/S0219749918500053.

[8] Nan Jiang and Luo Wang. "Quantum image scaling using nearest neighbor interpolation". In: *Quantum Information Processing* 14.5 (2015), pp. 1559–1571. ISSN: 1573-1332. DOI: 10.1007/s11128-014-0841-8.

[9] Nan Jiang, Jian Wang, and Yue Mu. "Quantum image scaling up based on nearest-neighbor interpolation with integer scaling ratio". In: *Quantum Information Processing* 14 (Aug. 2015). DOI: 10.1007/s11128-015-1099-5.

[10] Hai-Sheng Li, Ping Fan, Hai-Ying Xia, Huiling Peng, and Shuxiang Song. "Quantum Implementation Circuits of Quantum Signal Representation and Type Conversion". In: *IEEE Transactions on Circuits and Systems I: Regular Papers* 66.1 (2019), pp. 341–354. DOI: 10.1109/TCSI.2018.2853655.

[11] Sowmik Kanti Deb and W. David Pan. "Quantum Image Compression: Fundamentals, Algorithms, and Advances". In: *Computers* 13.8 (2024). DOI: 10.3390/computers13080185.

[12] Chao Pang, Zheng-Wei Zhou, and Guang-Can Guo. "A Hybrid Quantum Encoding Algorithm of Vector Quantization for Image Compression". In: *Chinese Physics* 15 (Apr. 2006). DOI: 10.1088/1009-1963/15/12/044.

[13] Chao Yang Pang, Zheng Wei Zhou, and Guang Can Guo. *Quantum Discrete Cosine Transform for Image Compression*. 2006. arXiv: quant-ph/0601043 [quant-ph].

[14] Ali Nodehi, Mohamad Tayarani, and Fariborz Mahmoudi. "A novel functional sized population quantum evolutionary algorithm for fractal image compression". In: *2009 14th International CSI Computer Conference*. 2009, pp. 564–569. DOI: 10.1109/CSICC.2009.5349639.

[15] Qi-gao Feng and Hao-yu Zhou. "Research of Image Compression Based on Quantum BP Network". In: *TELKOMNIKA Indonesian Journal of Electrical Engineering* 12 (July 2014). DOI: 10.11591/telkomnika.v12i1.3908.

[16] Songlin Du, Yaping Yan, and Yide Ma. "Quantum-Accelerated Fractal Image Compression: An Interdisciplinary Approach". In: *IEEE Signal Processing Letters* 22.4 (2015), pp. 499–503. DOI: 10.1109/LSP.2014.2363689.

[17] Nan Jiang, Xiaowei Lu, Hao Hu, Yijie Dang, and Yongquan Cai. "A Novel Quantum Image Compression Method Based on JPEG". In: *International Journal of Theoretical Physics* 57.3 (Mar. 2018), pp. 611–636. ISSN: 1572-9575. DOI: 10.1007/s10773-017-3593-2.

[18] Yan Ma and Nan-Run Zhou. "Quantum color image compression and encryption algorithm based on Fibonacci transform". In: *Quantum Information Processing* 22.1 (Jan. 2023), p. 39. ISSN: 1573-1332. DOI: 10.1007/s11128-022-03749-6.

[19] Hengyan Wang, Jing Tan, Yixiao Huang, and Wenqiang Zheng. "Quantum image compression with autoencoders based on parameterized quantum circuits". In: *Quantum Information Processing* 23.2 (Jan. 2024), p. 41. ISSN: 1573-1332. DOI: 10.1007/s11128-023-04243-3.

[20] Xun Ji, Qin Liu, Shan Huang, Andi Chen, and Shengjun Wu. *Image Compression and Reconstruction Based on Quantum Network*. 2024. arXiv: 2404.11994 [quant-ph].

[21] Norhan Nasr, Ahmed Younes, and Ashraf Elsayed. "Efficient representations of digital images on quantum computers". In: *Multimedia Tools and Applications* 80 (Oct. 2021). DOI: 10.1007/s11042-021-11355-4.

[22] Md Ershadul Haque, Manoranjan Paul, Anwaar Ulhaq, and Tanmoy Debnath. "Advanced quantum image representation and compression using a DCT-EFRQI approach". In: *Scientific Reports* 13 (Mar. 2023). DOI: 10.1038/s41598-023-30575-2.

[23] Robert K. Brayton, Gary D. Hachtel, Curtis T. McMullen, and Alberto L. Sangiovanni-Vincentelli. *Logic Minimization Algorithms for VLSI Synthesis*. Springer New York, NY, 1984. DOI: 10.1007/978-1-4613-2821-6.

[24] Rabia Khan. "An improved flexible representation of quantum images". In: *Quantum Information Processing* 18 (May 2019). DOI: 10.1007/s11128-019-2306-6.

[25] Rakesh Saini, Bikash K. Behera, Saif Al-Kuwari, and Ahmed Farouk. *NEQRX: Efficient Quantum Image Encryption with Reduced Circuit Complexity*. 2024. arXiv: 2204.07996 [quant-ph].

[26] Konstantinos Papakonstantinou and G. Papakonstantinou. "A Nonlinear Integer Programming Approach for the Minimization of Boolean Expressions". In: *Journal of Circuits, Systems and Computers* 27 (Jan. 2018), p. 1850163. DOI: 10.1142/S0218126618501633.

[27] George Papakonstantinou. "A parallel algorithm for minimizing ESOP expressions". In: *Journal of Circuits, Systems and Computers* 23 (Feb. 2014). DOI: 10.1142/S0218126614500157.

[28] Bernd Becker, Rolf Drechsler, and Michael Theobald. "Minimization of 2-level AND/XOR Expressions using Ordered Kronecker Functional Decision Diagrams". In: (May 1994).

[29] Alan Mishchenko and Marek Perkowski. "Fast Heuristic Minimization of Exclusive-Sums-of-Products". In: *5th International Reed-Muller Workshop* (Sept. 2001).

[30] Jae-Seung Lee, Yongwook Chung, Jaehyun Kim, and Soonchil Lee. *A Practical Method of Constructing Quantum Combinational Logic Circuits*. 1999. arXiv: quant-ph/9911053 [quant-ph].

[31] Shahab Iranmanesh, Randa Atta, and Mohammad Ghanbari. "Implementation of a quantum image watermarking scheme using NEQR on IBM quantum experience". In: *Quantum Information Processing* 21.6 (2022), p. 194. ISSN: 1573-1332. DOI: 10.1007/s11128-022-03530-9.

[32] Adriano Barenco, Charles H. Bennett, Richard Cleve, David P. DiVincenzo, Norman Margolus, Peter Shor, Tycho Sleator, John A. Smolin, and Harald Weinfurter. "Elementary gates for quantum computation". In: *Physical Review A* 52 (1995), pp. 3457–3467. DOI: 10.1103/PhysRevA.52.3457.

[33] Malgorzata Chrzanowska-jeske, Alan Mishchenko, and Marek Perkowski. "Generalized Inclusive Forms; New Canonical Reed-Muller Forms Including Minimum ESOPs". In: *VLSI Design* 14 (Feb. 2002). DOI: 10.1080/10655140290009774.

[34] Faraj Khalid. "Combinational logic synthesis based on the dual form of Reed-Muller representation". PhD thesis. Edinburgh Napier University, 2005.

[35] Valentin Bakoev and Krassimir Manev. "Fast computing of the positive polarity Reed-Muller transform over GF (2) and GF (3)". In: *Eleventh International Workshop on Algebraic and Combinatorial Coding Theory* (June 2008), pp. 13–21.

[36] *USC-SIPI Image Database*. https://sipi.usc.edu/database Accessed on: Aug. 5, 2024.